Probing Single-Cell Micromechanics In Vivo: The Microrheology of *C. elegans* Developing Embryos

Brian R. Daniels,* Byron C. Masi,* and Denis Wirtz*†‡
*Department of Chemical and Biomolecular Engineering, †Department of Materials Science and Engineering, ‡Howard Hughes Medical Institute Graduate Program, The Johns Hopkins University, Baltimore, Maryland

ABSTRACT Cells are not directly accessible in vivo and therefore their mechanical properties cannot be measured by methods that require a direct contact between probe and cell. Here, we introduce a novel in vivo assay based on particle tracking microrheology whereby the extent and time-lag dependence of the mean squared displacements of thermally excited nanoparticles embedded within the cytoplasm of developing embryos reflect local viscoelastic properties. As a proof of principle, we probe local viscoelastic properties of the cytoplasm of developing *Caenorhabditis elegans* embryos. Our results indicate that unlike differentiated cells, the cytoplasm of these embryos does not exhibit measurable elasticity, but is highly viscous. Furthermore, the viscosity of the cytoplasm does not vary along the anterior-posterior axis of the embryo during the first cell division. These results support the hypothesis that the asymmetric positioning of the mitotic spindle stems from an asymmetric distribution of elementary force generators as opposed to asymmetric viscosity of the cytoplasm.

INTRODUCTION

Current cell mechanics methods—atomic force microscopy (AFM) (1), micropipette suction (2,3), parallel plates (4), magnetic bead twisting (5), and cell poking (6)—require a direct contact between the cell surface and the physical probe to extract the rheological parameters that describe the mechanical properties of the cell. However, cells in their physiological environment are largely inaccessible to mechanical probes because they are often organized within an extracellular matrix and buried in soft and solid tissues. Furthermore, the developing embryos of many organisms are housed within rigid shells, making them inaccessible to physical probes. Therefore, to test the fundamental biophysical properties of cells in their physiological milieu, there is a need to develop a biophysical method that does not require direct contact with the cell surface to obtain information about the mechanical state of cells in vivo.

We have introduced and refined the method of particle tracking microrheology, whereby the Brownian displacements of individual submicron particles embedded in a complex fluid (such as the cytoplasm of living cells) are monitored simultaneously with high spatial and temporal resolution (7–10). The extent and time lag-dependence of the mean squared displacements (MSDs) of the nanoparticles directly reflect the local micromechanical properties of the viscoelastic milieu in the vicinity of each nanoparticle (11). The method of particle tracking microrheology has been used to probe the intracellular mechanical response of living cells exposed in vitro to migratory cues (12), the topical addition of actin filament cross-linkers (10), shear flow stimuli (13), and agonists of actomyosin contractility (14).

Although this approach does not require direct contact between the cell and the probe, its current form does not make it readily amenable to probe the microrheology of cells in vivo. Indeed, to circumvent the endocytic pathway involving the directed motion of nanoparticles in endocytic vesicles, nanoparticles must be introduced directly (usually via microinjection) into the cytoplasm of the cells, which is not immediately possible. Here, we adapt the method of particle tracking microrheology to probe, for the first time, the mechanical properties of the cytoplasm of individual cells in vivo. To establish a proof of principle, we determine the local time-dependent viscoelastic properties of the cytoplasm of developing *Caenorhabditis elegans* zygotes undergoing polarization. *C. elegans*, a small free-living nematode, is used extensively as a model organism in many areas of current biological research, notably cellular polarization. Probing the viscoelastic properties of a viable, developing *C. elegans* embryo is challenging, as it is enclosed in an impermeable shell throughout its early development, making it impossible to probe using conventional biophysical methods. The biophysical properties therein have implications in many aspects of the polarization process from mitotic spindle positioning to the transport of subcellular organelles.

Cellular polarization is a highly regulated process marked by the asymmetric distribution of intracellular constituents. The ability to attain a polarized state is essential for the proper function of virtually all differentiated cells and operates under highly conserved mechanisms. Despite the importance and diverse context of cell polarity, relatively little is known about the physical phenomena that mediate this phenomenon. The *C. elegans* zygote represents a popular

Submitted December 30, 2005, and accepted for publication February 24, 2006.

Address reprint requests to Denis Wirtz, Dept. of Chemical and Biomolecular Engineering, The Johns Hopkins University, 3400 N. Charles St., Baltimore, MD 21218. Tel.: 410-516-7006; Fax: 410-516-5510; E-mail: wirtz@jhu.edu.

0006-3495/06/06/4712/08 $2.00

doi: 10.1529/biophysj.105.080606

model system for the study of natural cellular polarization due to the fact that the first few polarized cleavages determine the ultimate body axes of the adult organism (15). Furthermore, the relative ease of genetic manipulations, such as gene transgenic expression and gene silencing via RNAi (16), provide the opportunity to explore the roles of individual genes in the polarization process.

The polarization of the *C. elegans* embryo is initiated upon fertilization by a cue from the incoming sperm, whose point of entry determines the ultimate posterior pole of the embryo (17). The embryo becomes polarized along the anterior/posterior (A/P) axis by cytoskeletal-mediated mechanisms (18–20). Asymmetric contractility of the cortical actin meshwork generates large-scale cytoplasmic flow, whereby internal cytoplasm flows toward the posterior pole and cortical cytoplasm flows reciprocally toward the anterior pole of the embryo, resulting in both cortical and cytoplasmic reorganization before the first cell cleavage (20,21). Several constituents of the cytoplasm, including members of the Par family of proteins (22,23) and germ granules (24,25), are asymmetrically segregated during distinct polarization phases (26). Subsequent cytokinesis at the eccentrically positioned mitotic spindle generates two daughter cells—a somatic blastomere at the anterior and a germline progenitor at the posterior, which differ in size, cellular endowment, and differentiation potential (15,27).

Asymmetric cell division is crucial for the generation of cell diversity in developing organisms. During anaphase of the initial mitosis in the *C. elegans* embryo, the mitotic spindle elongates asymmetrically, whereby the anterior spindle pole remains relatively stationary and the posterior spindle pole is displaced posteriorly as it oscillates transversely (28). Cytokinesis about the asymmetric spindle results in a posterior blastomere smaller than that of the anterior. In previous studies, the mitotic spindle was severed by various methods and the resultant motion of the spindle poles was monitored (29). These studies revealed the striking effect that the posterior spindle pole traveled through the embryonic cytoplasm at a higher peak velocity than its anterior counterpart. Possible explanations for this phenomenon include either a difference in the net force acting on each spindle pole, a difference in the viscoelastic properties of the cytoplasm through which each spindle pole travels, or both. To address these possibilities, the viscoelastic properties of the *C. elegans* embryo were characterized using in vivo particle tracking microrheology.

Results from the in vivo microrheology studies presented here indicate that the embryonic cytoplasm behaves as a highly viscous liquid with negligible elasticity. Despite large morphological changes and continuous cytoskeleton reorganization, the properties of the cytoplasm of the *C. elegans* embryo remain spatially uniform throughout the embryo from fertilization until the two-cell stage. Due to the fact that migrating subcellular structures of equivalent size and shape encounter equal viscous drag, the results safely rule out the possibility that differences in viscoelastic properties mediate physical asymmetries present in the first embryonic division. Therefore, our results support the hypothesis that the asymmetric positioning of the mitotic spindles derives from the asymmetric distribution of forces, as opposed to asymmetric viscoelastic properties within the zygote (30). Furthermore, using the absolute value of the cytoplasmic viscosity determined from in vivo particle tracking microrheology, we estimate the force exerted by a single elementary force generator to be in the single-piconewton scale, supporting the hypothesis that the mitotic spindles are pulled cortically by minus end-directed dynein motor proteins (31).

MATERIALS AND METHODS

C. elegans strain maintenance

We used the *C. elegans* strain derived from the wild-type Bristol strain N2. It was cultured as described (32), except that worms were maintained at 25°C.

Light microscopy

Young *C. elegans* eggs were obtained by cutting gravid hermaphrodites worms in egg salts (118 mM NaCl, 121 mM KCl in H_2O) with the help of a dissecting microscope and transferred to 3% agarose pads (Invitrogen, Carlsbad, CA) sealed by capillary action underneath cover slips (VWR, West Chester, PA). Eggs were viewed by DIC optics using a Nikon TE300 epifluorescence microscope with a 60× DIC oil-immersion lens (N.A. 1.4, Nikon, Melville, NY) and an Orca II charge-coupled device camera (Hamamatsu; Bridgewater, NJ). All image collection was performed at 25°C.

Preparation of PEG-coated nanoparticles

To probe the micromechanical properties of live embryos, we used primarily polyethylene glycol (PEG) coated (PEGylated) 100-nm diameter nanoparticles, which were prepared as described (33). Briefly, 5 mg/ml amine-terminated PEG (diamino-PEG, average MW 3400) (Shearwater, Huntsville, AL) in 50 mM MES (pH = 6.0) was mixed at 1:1 ratio with 2% w/v aqueous suspension of carboxylate-modified polystyrene nanoaparticles (Molecular Probes, Eugene, OR) and incubated for 15 min at room temperature. Then 1-ethyl-3-(3-dimethylaminopropyl)-carbodiimide (EDAC) was added to a final concentration of 4 mg/mL and the pH was adjusted to 6.5. The resulting solution was incubated overnight. 100 mM glycine was added to quench the reaction and the mixture was incubated for 30 min at room temperature. PEGylated microspheres were obtained by centrifugation (3,300 g for 15 min) and washed three times with PBS.

Incorporation of nanoparticles in *C. elegans* embryos

A colloidal suspension of fluorescent polystyrene nanoparticles was dialyzed against ddH_2O overnight at room temperature. The nanoparticles were surface-modified with the hydrophilic polymer PEG to ensure that the nanoparticles did not interact directly with subcellular structures. Microneedles (World Precision Instruments, Sarasota, FL) pulled on a vertical micropipette puller (Sutter Instruments, Novato, CA) (34) were filled by capillary action with the nanoparticle suspension. The needles were mounted on a microinjector controlled by a micromanipulator (Eppendorf 5170, Hamburg, Germany) mounted on a Zeiss Axiovert 10 inverted microscope (Zeiss, Germany). The nanoparticles were microinjected into the syncytial

gonads of gravid hermaphrodites according to the protocol developed for transformation (35). After injection, worms were immersed in recovery buffer (20% glucose, 1M KCl, 5M NaCl, 1M $MgCl_2$, 1M $CaCl_2$, 1M HEPES pH 7.2 in H_2O) for at least 15 min and then transferred to M9 buffer (22mM KH_2PO_4, 42mM Na_2HPO_4, 85mM NaCl, 1mM $MgSO_4$ in H_2O) for at least 1 h before being incubated at 25°C for ~4 h before image acquisition.

Particle-tracking intracellular microrheology

The motion of fluorescent nanoparticles embedded in the cytoplasm of embryos was recorded at a rate of 30 frames/second using a silicon-intensifier target (SIT) camera (VE-100 Dage-MTI, Michigan City, IN) mounted on a Nikon TE300 epifluorescence microscope with a 60× DIC oil-immersion lens (N.A. 1.4, Nikon). DIC images of the embryos were acquired with an Orca II charge-coupled device camera (Hamamatsu) between acquisitions movies of nanoparticle movements. Image acquisition was performed at 25°C.

Movies of nanoparticle motion were analyzed using Metamorph software (Universal Imaging, West Chester, PA) and custom software designed to transform MSD into rheological parameters describing the viscoelastic properties of the cytoplasm (14). The displacement of the intensity-weighted centroid of each nanoparticle was tracked with a resolution of ~10 nm. This spatial resolution on displacement was measured independently by tethering nanoparticles to a glass cover slip and measure their apparent displacement, as described (9). The coordinates of the centroids were transformed into time-averaged mean squared displacements MSDs:

$$\langle \Delta r^2(\tau) \rangle = \langle [x(t+\tau) - x(t)]^2 + [y(t+\tau) - y(t)]^2 \rangle.$$

Here t is the elapsed time and τ is the time lag. We verified that $\langle [x(t+\tau) - x(t)]^2 \rangle = \langle [y(t+\tau) - y(t)]^2 \rangle$, which indicates that the embryos were locally isotropic. The two-demensional MSD in a viscous medium (i.e., no elasticity) depends linearly on time lag:

$$\langle \Delta r^2(\tau) \rangle = 4D\tau,$$

where D is the diffusion coefficient of the nanoparticles of radius $a = 50$ nm. The diffusion coefficient is related to the viscosity of the suspending milieu, η, by the Stokes-Einstein relationship (36):

$$D = k_B T / 6\pi\eta a.$$

Further details about the multiple-particle tracking and microrheology analysis, including effects of particle sizes and surface chemistry, have been presented previously (10,37).

RESULTS

Incorporation of inert nanoparticles in *C. elegans* embryos

To probe the viscoelastic properties of developing *C. elegans* embryos, we injected small inert nanoparticles of known size, shape, and surface chemistry into the reproductive system of adult organisms. Based on a general microinjection protocol developed for *C. elegans* transformation (16), we injected an aqueous colloidal suspension of nanoparticles into the syncytial gonad of gravid hermaphrodites (Fig. 1 *A*). The gonad plasm, containing the injected nanoparticles, ultimately became incorporated into the cytoplasm of nascent oocytes, which were then fertilized and enclosed within an impermeable shell.

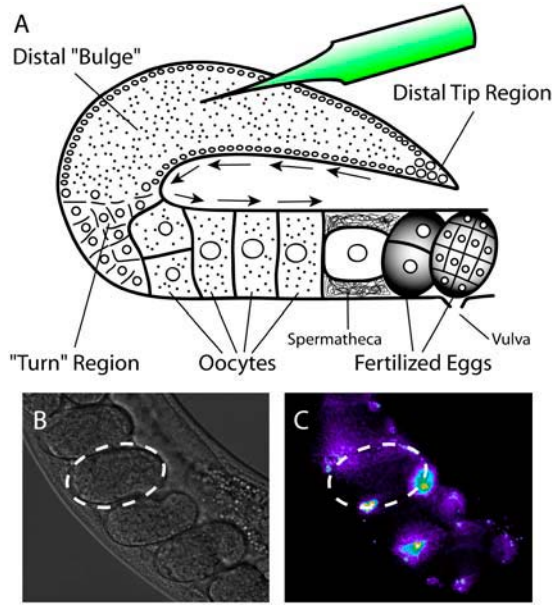

FIGURE 1 Incorporation of nanoparticles into the cytoplasm of developing *C. elegans* embryos. (*A*) An aqueous suspension of nanoparticles was injected into the gonad of gravid adult organisms. The nanoparticles were incorporated into the cytoplasm of nascent oocytes, which were fertilized and enclosed within an impermeable shell (*gray*) at the spermatheca. The resulting embryos containing a uniform dispersion of nanoparticles were excised and subjected to fluorescence microscopy. Diameter of nanoparticles, 100 nm. (*B*, DIC; *C*, fluorescence) COOH-modified nanoparticles interact with the walls of the gonad, resulting in embryos (*dashed lines*) containing a relatively small percentage of the injected nanoparticles.

To maximize the efficiency of the injection procedure (number of nanoparticles per injected worm), we tested nanoparticles of various surface chemistries. Carboxylate-modified nanoparticles (COOH-nanoparticles) were incorporated into developing embryos. However, presumably due to their tendency to interact with various biomolecules, COOH-nanoparticles aggregated at the walls of the gonad rather than remaining suspended in plasm (Fig. 1, *B* and *C*). To circumvent this problem, we generated polyethylene-glycol-modified nanoparticles (PEG-nanoparticles), which are effectively inert and electrostatically neutral. These PEG-nanoparticles remained suspended in plasm, significantly increasing in the overall efficiency of the injection process. Furthermore, the use of inert PEG-nanoparticles greatly decreased the propensity of these particles to become coupled to macromolecular structures within developing embryos, such as mitotic apparatus or cortical cytoskeletal networks. Indeed, we were able to incorporate a relatively large number of uniformly dispersed PEG-nanoparticles into single embryos (Fig. 2, *A* and *B*). The viability of developing embryos containing PEG-nanoparticles was monitored with DIC optics until at least the eight-cell stage. The injection procedure had no observable effect on developing embryos, which continued to develop normally into post-embryonic stages (Fig. 2, *C* and *D*).

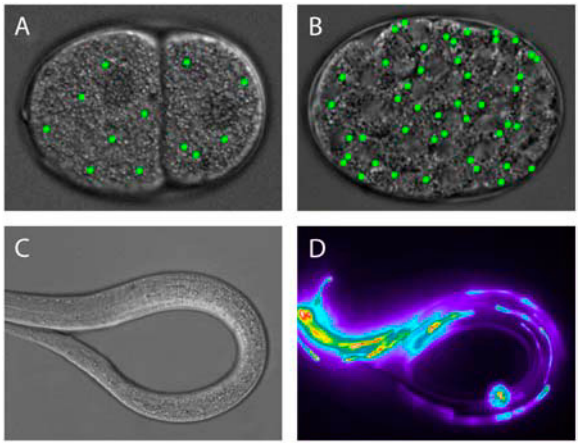

FIGURE 2 Inert nanoparticles remain uniformly dispersed throughout all stages of growth. (*A*) PEG-nanoparticles do not become enriched in either the anterior or posterior blastomeres after the first embryonic division. (*B*) The nanoparticles remain uniformly distributed through later stages of embryonic development (*C* and *D*), and can be found in newly-hatched L1 animals (*C*).

High-resolution tracking of inert nanoparticles in *C. elegans* embryos

Embryos containing PEG-nanoparticles were extracted from the adult worms and their biophysical properties probed using time-resolved fluorescent microscopy. We restricted our investigation of these properties to the early embryo, from fertilization until the two-cell stage (Fig. 2 *A*), to address the means by which daughter blastomeres of unequal size are generated during the first cell division.

Trajectories of the centroids of nanoparticles embedded within the anterior and posterior cytoplasm of early *C. elegans* embryos were monitored with 10-nm spatial resolution and 33-ms temporal resolution for 20-s intervals (Fig. 3, *A* and *B*). The dependence of particle mean squared displacements (MSDs) on the time-lag, τ, was used to infer the local viscoelastic properties of cytoplasmic cytoplasm. The MSD, $\langle \Delta r^2(\tau) \rangle$, of a spherical particle undergoing thermal motion in a complex fluid exhibits a dependence on time-lag modeled as $\langle \Delta r^2(\tau) \rangle \sim \tau^{\alpha}$. In a simple viscous fluid, $\alpha = 1$ and the MSD exhibits a linear dependence on the time lag. In a fluid that exhibits elasticity, particle motion becomes restricted and demonstrates subdiffusive behavior, described by $\alpha < 1$ and a MSD that grows more slowly with time lag. Conversely, the MSDs of particles experiencing convective flow grow more rapidly with time, described by $\alpha > 1$. For example, in the presence of a linear velocity field with constant velocity, v, the displacement of a particle over a time-lag, τ, is described by $r = v\tau$, resulting in a MSD of $\langle \Delta r^2(\tau) \rangle = (v\tau)^2$, where $\alpha = 2$. However, due to the fact that velocity fields in biological systems are often transient and nonuniform, MSDs rarely attain α-values as high as 2. The slope of a log-log plot of MSDs as a function of time-lag indicates the α-value.

The embryonic cytoplasm is highly viscous and symmetric throughout the first cell division

The MSDs of inert nanoparticles embedded within the embryonic cytoplasm indicated predominantly viscous diffusion over a relatively narrow range of displacements in both the anterior and posterior cytoplasm (Fig. 3, *C* and *D*). Indeed, these MSDs grow approximately linearly with time-lag showing a narrow range of slopes. The MSDs began to display convective behavior at longer time-lags ($\tau > 1$s), indicating directed motion presumably due to bulk embryonic reorganization. There was also a considerable lack of subdiffusive particles, making the elasticity of the cytoplasm too small to measure. MSDs in both the anterior and posterior cytoplasm had narrow distributions about the mean (Fig. 3, *E* and *F*), indicating that the viscoelastic properties of the embryonic cytoplasm were largely uniform throughout the embryo. The difference between the MSDs of nanoparticles in the anterior and posterior was not statistically significant (unpaired student *t*-test, $P > 0.5$). The viscoelastic character of the embryonic cytoplasm did not vary with time, but remained constant throughout the first cell cycle (data not shown).

To directly compare the viscoelastic properties of the anterior and posterior regions, we determined the time-dependent ensemble averaged MSDs of each population (Fig. 4, *A* and *B*). These global averages showed that the viscoelastic character of the cytoplasm in each region was virtually identical over all time-lags considered. Because the nanoparticles behaved as colloidal spheres undergoing Brownian motion in a simple viscous fluid, their two-dimensional ensemble averaged MSDs can be described by $\langle \Delta r^2(\tau) \rangle = 4D\tau$, where D is the effective diffusion coefficient. This relationship provided an excellent fit for both sets of data ($R^2 > 0.98$ for anterior and posterior). The diffusion coefficients in the anterior and posterior regions were determined to be 0.0041 ± 0.0002 and 0.0040 ± 0.0002, respectively (mean $\pm$ SE) (Fig. 4 *C*). The diffusion coefficient of the beads in the anterior cytoplasm was ~3% greater than those in the posterior, within the range of experimental error.

Using the Stokes-Einstein equation, $D = k_B T/6\pi\eta a$, which relates the mean diffusion coefficient of a spherical Brownian particle to the viscosity of its suspending medium (Fig. 4 *A*), we determined that the mean shear cytoplasmic viscosity in the anterior and posterior regions of *C. elegans* early embryos to be $\eta = 10.3 \pm 0.8$ Poise and 10.7 ± 0.8 Poise, respectively (mean $\pm$ SE; 1 Poise = 0.1 Pascal $\times$ s) (Fig. 4 *D*). Here k_B is Boltzmann's constant, T is the absolute temperature, and $a = 50$ nm is the radius of the nanoparticle. Therefore, the viscosity of the early embryo is ~3 orders of magnitude greater than that of water (0.01 Poise) and similar to that of glycerin.

DISCUSSION

We extended the method of particle tracking microrheology to probe the viscoelastic properties of the *C. elegans* early

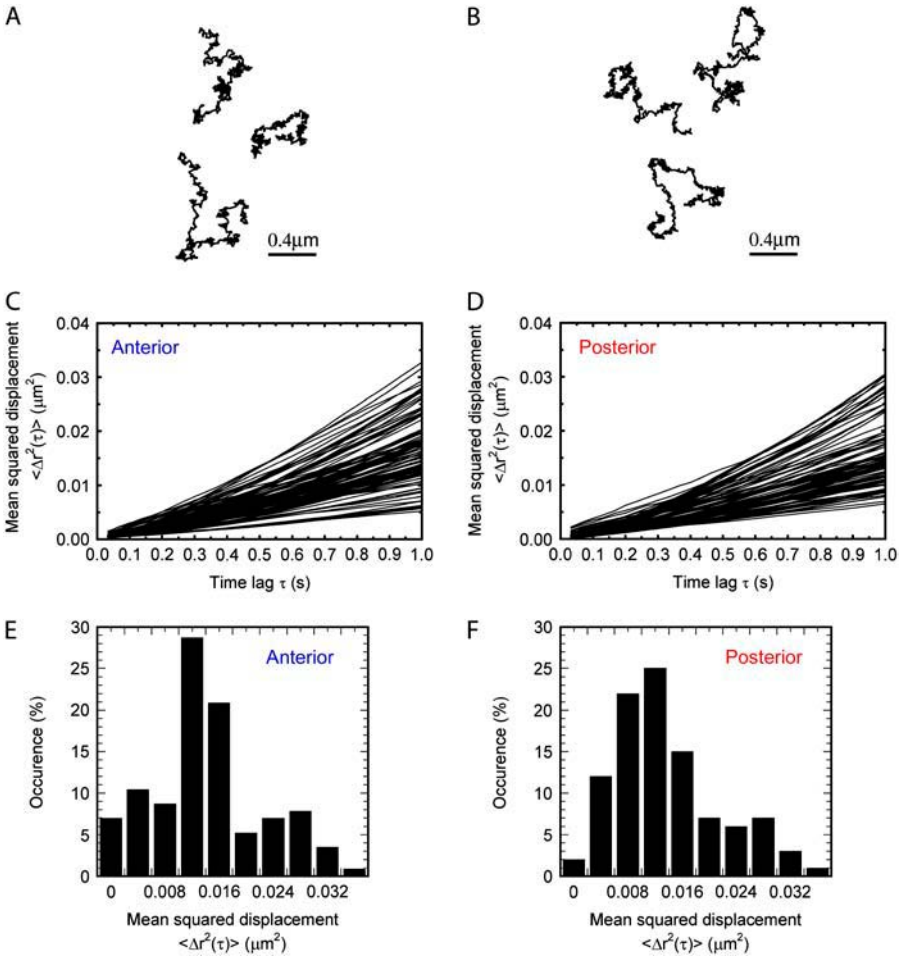

FIGURE 3 Mean-squared displacements of nanoparticles in anterior/posterior (A/P). (*A* and *B*) Typical trajectories of the centroids of PEG-nanoparticles embedded within the anterior and posterior cytoplasm exhibit random-walks characteristic of viscous diffusion. (*C* and *D*) MSDs of individual nanoparticles exhibit an approximately linear dependence with time-lag over a narrow distribution of slopes. (*E* and *F*) Displacements of PEG-nanoparticles exhibit a relatively narrow distribution about the mean value.

embryo. The rheological properties of the embryonic cytoplasm differ significantly from those of the cytoplasm of various differentiated cell types, including mouse 3T3 cells, human endothelial cells, and mouse epithelial cells (12,14, 38,39) (see Table 1). The cytoplasm of these differentiated cell types behaves much like an elastic gel, whereas the embryonic cytoplasm lacks measurable elasticity. Because the elasticity of differentiated cells is mediated mostly by the actin cytoskeleton (8), it is unlikely that actin microfilaments confer any mechanical integrity to the internal cytoplasm of *C. elegans* embryos. Indeed, immunofluorescence visualization of actin in the early embryo shows that actin is concentrated about the cortex of the embryo, leaving the cytoplasm largely devoid of rigid actin structures (40).

Our results indicate that the embryonic cytoplasm exhibits high viscosity with negligible elasticity and, from a rheological standpoint, remains spatially uniform throughout the first cell cycle. These findings support the hypothesis that the asymmetric positioning of the mitotic spindle is driven by an imbalance in the net force exerted on the spindle rather than asymmetric viscous drag encountered by the migrating spindle poles (29). The source of the force imbalance was studied by ablating centrosomes via optically-induced centrosome disintegration (OICD) and monitoring the motion of the resulting centrosome fragments. The mean and variance of fragment velocities were used to infer that the force imbalance is caused by a nonuniform distribution of identical elementary force generators, each contributing an elementary force of f_e when in the active state. Although the results yielded the elementary velocity due to a single force generator, v_e, the drag coefficient associated with centrosome fragments movements in the cytoplasm could not be determined without the absolute magnitude of the cytoplasmic viscosity. Therefore, the absolute value of the elementary force exerted by a single force generator could not be determined.

Using Stokes' law, $f_e = \xi\, v_e$, where $\xi = 6\pi\eta R$ is the viscous drag coefficient, to model the viscous drag encountered by centrosomes fragments, we calculated the elementary force, f_e, to be ~5 piconewtons (pN). This force is ~5× greater than the elementary force generated by dynein, a microtubule motor protein (31). However, it is likely that fragment sizes, R, measured by fluorescence microscopy, were overestimated by at least the same factor (S.W. Grill, personal correspondence). Therefore, our findings support the model in which minus-end-directed dyneins mediate spindle positioning in the early embryo.

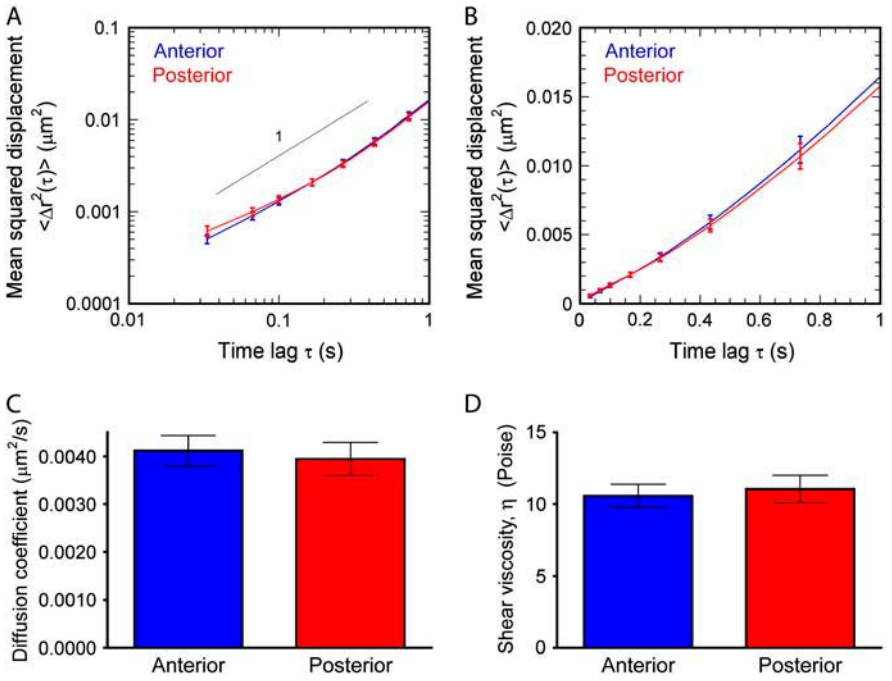

FIGURE 4 Ensemble averaged MSDs, mean diffusion coefficient of nanoparticles and viscosity of early embryonic cytoplasm. (*A*, log-log; *B*, linear) Ensemble averaged MSDs of the anterior and posterior populations of cytoplasmic PEG-nanoparticles are nearly identical and exhibit predominantly viscous character with the slight influence of convective flow at long time-lags. The linear constant (slope) of the linear relationship reflects the diffusive properties of the nanoparticles within the cytoplasm. (*C*) The bulk diffusion coefficients, *D*, of nanoparticles within the anterior and posterior cytoplasm were determined to be 0.0041 ± 0.002 and 0.0040 ± 0.0002, respectively. (*D*) The effective shear viscosity, inversely related to the diffusion coefficient, of the anterior and posterior cytoplasm was determined to be 10.3 ± 0.8, and 10.7 ± 0.8 Poise, respectively, ~3 orders of magnitude higher than that of water. Reported values represent mean ± SE.

The absolute magnitude of the cytoplasmic viscosity may be used to determine the force necessary to transport subcellular organelles and macromolecular complexes, such as pronuclei or germ granules, through the cytoplasm during embryonic reorganization and patterning. Because migrating organelles must, at the very least, overcome the viscous drag encountered due to their motion, the viscosity effectively sets a lower bound for the force transduction necessary for such motion. However, the α-values that exceed 1 at increasing time-lags indicate the presence of convection within the cytoplasm, presumably due to cytoplasmic streaming. Subcellular organelles and macromolecular structures may depend on this flow rather than molecular motors as a means of migration. It should be noted, however, that despite the presence of these cytoplasmic velocity fields, the inert nanoparticles remained uniformly dispersed throughout the embryos (Fig. 2, *A* and *B*), indicating that cytoplasmic flow is not sufficient to segregate submicron particles.

Together, these results show the new possibility of probing single-cell mechanics in vivo, where the physical

TABLE 1 Elasticity and shear viscosity of the cytoplasm of different types of cells.

	Average viscosity (Poise)	Average elasticity at 1 Hz (dyne/cm^2)	Reference
Single-cell *C. elegans* embryo	10 ± 1	negligible	This work
Serum-starved Swiss3T3 fibroblast*	10 ± 3	50 ± 20	Kole et al. (14)
Serum-starved Swiss 3T3 fibroblast treated with LPA†	95 ± 20	120 ± 30	Kole et al. (14)
Serum-starved Swiss3T3 fibroblast subjected to shear flow‡	300 ± 40	600 ± 50	Lee et al. (13)
Swiss 3T3 fibroblast at the edge of a wound§	45 ± 15	330 ± 30	Kole et al. (12)
Mouse embryonic fibroblast (MEF)¶	18 ± 2	140 ± 30	J. S. H. Lee, P. Panorchan, and D. Wirtz, unpublished
HUVEC‖	17 ± 1	130 ± 10	J. S. H. Lee, P. Panorchan, and D. Wirtz, unpublished

All reported viscosity and elasticity were obtained by particle tracking microrheology. All measurements are mean ± SE. Unit conversions are 1 dyne/cm^2 = 0.1 Pa = 0.1 N/m^2 = 0.1 pN/μm^2. Pa, Pascal; pN, piconewton.

*Cells placed on fibronectin deposited on glass were serum starved for 48 h before measurements.

†Serum-starved cells placed on fibronectin deposited on glass were treated with lysophosphatidic acid (LPA), which was applied 15 min before measurements.

‡Cells were grown on fibronectin and exposed for 40 min to shear flow before measurements.

§Cells in complete medium and grown on fibronectin to confluence were wounded to induce migration.

¶Cells in complete medium and plated on glass.

‖Cells in complete medium and plated on a peptide hydrogel.

properties of individual cells are probed in live animals. Another possible approach to measure cell mechanics in embryos would consist in injecting magnetic beads, instead of inert nanoparticles, into the gonad of *C. elegans*. Upon incorporation of the magnetic beads in the cytoplasm of embryo, its viscoelastic properties could be measured using magnetic tweezers (41,42), but this approach remains to be demonstrated.

The authors thank Stephan Grill for helpful discussions as well as Geraldine Seydoux, Michael L. Stitzel, and Cynthia DeRenzo for invaluable advice and technical assistance.

This work was funded by the National Aeronautics and Space Administration grant NAG9-1563, the National Institutes of Health grants GM065835 and GM075305, and a Howard Hughes Medical Institute graduate training grant in nanobiotechnology at Johns Hopkins.

REFERENCES

1. Hoh, J. H., and C. A. Schoenenberger. 1994. Surface morphology and mechanical properties of MDCK monolayers by atomic force microscopy. *J. Cell Sci.* 107:1105–1114.
2. Evans, E., K. Ritchie, and R. Merkel. 1995. Sensitive force technique to probe molecular adhesion and structural linkages at biological interfaces. *Biophys. J.* 68:2580–2587.
3. Merkel, R., R. Simson, D. A. Simson, M. Hohenadl, A. Boulbitch, E. Wallraff, and E. Sackmann. 2000. A micromechanic study of cell polarity and plasma membrane cell body coupling in Dictyostelium. *Biophys. J.* 79:707–719.
4. Thoumine, O., and A. Ott. 1997. Time scale dependent viscoelastic and contractile regimes in fibroblasts probed by microplate manipulation. *J. Cell Sci.* 110:2109–2116.
5. Wang, N., J. P. Butler, and D. E. Ingber. 1993. Mechanotransduction across the cell surface and through the cytoskeleton. *Science.* 260: 1124–1127.
6. Duszyk, M., B. Schwab, G. I. Zahalak, H. Qian, and E. L. Elson. 1989. Cell poking: quantitative analysis of indentation of thick viscoelastic layers. *Biophys. J.* 55:683–690.
7. Mason, T. G., K. Ganesan, J. V. van Zanten, D. Wirtz, and S. C. Kuo. 1997. Particle-tracking microrheology of complex fluids. *Phys. Rev. Lett.* 79:3282–3285.
8. Yamada, S., D. Wirtz, and S. C. Kuo. 2000. Mechanics of living cells measured by laser tracking microrheology. *Biophys. J.* 78:1736–1747.
9. Apgar, J., Y. Tseng, E. Federov, M. B. Herwig, S. C. Almo, and D. Wirtz. 2000. Multiple-particle tracking measurements of heterogeneities in solutions of actin filaments and actin bundles. *Biophys. J.* 79: 1095–1106.
10. Tseng, Y., T. P. Kole, and D. Wirtz. 2002. Micromechanical mapping of live cells by multiple-particle-tracking microrheology. *Biophys. J.* 83:3162–3176.
11. Xu, J., V. Viasnoff, and D. Wirtz. 1998. Compliance of actin filament networks measured by particle-tracking microrheology and diffusing wave spectroscopy. *Rheologica Acta.* 37:387–398.
12. Kole, T. P., Y. Tseng, I. Jiang, J. L. Katz, and D. Wirtz. 2005. Intracellular mechanics of migrating fibroblasts. *Mol. Biol. Cell.* 16: 328–338.
13. Lee, J. S. H., P. Panorchan, C. M. Hale, S. B. Khatau, Y. Tseng, and D. Wirtz. 2006. Shear flow induces cytoplasmic stiffening as revealed by ballistic intracellular nanorheology. *J. Cell Sci.* 116:1760–1768.
14. Kole, T. P., Y. Tseng, L. Huang, J. L. Katz, and D. Wirtz. 2004. Rho kinase regulates the intracellular micromechanical response of adherent cells to rho activation. *Mol. Biol. Cell.* 15:3475–3484.
15. Hyman, A. A., and J. G. White. 1987. Determination of cell division axes in the early embryogenesis of *Caenorhabditis elegans*. *J. Cell Biol.* 105:2123–2135.
16. Fire, A., S. Xu, M. K. Montgomery, S. A. Kostas, S. E. Driver, and C. C. Mello. 1998. Potent and specific genetic interference by double-stranded RNA in *Caenorhabditis elegans*. *Nature.* 391:806–811.
17. Goldstein, B., and S. N. Hird. 1996. Specification of the anteroposterior axis in *Caenorhabditis elegans*. *Development.* 122:1467–1474.
18. Malone, C. J., L. Misner, N. Le Bot, M. C. Tsai, J. M. Campbell, J. Ahringer, and J. G. White. 2003. The *C. elegans* hook protein, ZYG-12, mediates the essential attachment between the centrosome and nucleus. *Cell.* 115:825–836.
19. Wallenfang, M. R., and G. Seydoux. 2000. Polarization of the anterior-posterior axis of *C. elegans* is a microtubule-directed process. *Nature.* 408:89–92.
20. Munro, E., J. Nance, and J. R. Priess. 2004. Cortical flows powered by asymmetrical contraction transport PAR proteins to establish and maintain anterior-posterior polarity in the early *C. elegans* embryo. *Dev. Cell.* 7:413–424.
21. Hird, S. N., and J. G. White. 1993. Cortical and cytoplasmic flow polarity in early embryonic cells of *Caenorhabditis elegans*. *J. Cell Biol.* 121:1343–1355.
22. Boyd, L., S. Guo, D. Levitan, D. T. Stinchcomb, and K. J. Kemphues. 1996. PAR-2 is asymmetrically distributed and promotes association of P granules and PAR-1 with the cortex in *C. elegans* embryos. *Development.* 122:3075–3084.
23. Lyczak, R., J. E. Gomes, and B. Bowerman. 2002. Heads or tails: cell polarity and axis formation in the early *Caenorhabditis elegans* embryo. *Dev. Cell.* 3:157–166.
24. Hird, S. N., J. E. Paulsen, and S. Strome. 1996. Segregation of germ granules in living *Caenorhabditis elegans* embryos: cell-type-specific mechanisms for cytoplasmic localisation. *Development.* 122: 1303–1312.
25. Hird, S. 1996. Cortical actin movements during the first cell cycle of the *Caenorhabditis elegans* embryo. *J. Cell Sci.* 109:525–533.
26. Cuenca, A. A., A. Schetter, D. Aceto, K. Kemphues, and G. Seydoux. 2003. Polarization of the *C. elegans* zygote proceeds via distinct establishment and maintenance phases. *Development.* 130: 1255–1265.
27. Bowerman, B., and C. A. Shelton. 1999. Cell polarity in the early *Caenorhabditis elegans* embryo. *Curr. Opin. Genet. Dev.* 9:390–395.
28. Albertson, D. G. 1984. Formation of the first cleavage spindle in nematode embryos. *Dev. Biol.* 101:61–72.
29. Grill, S. W., P. Gonczy, E. H. Stelzer, and A. A. Hyman. 2001. Polarity controls forces governing asymmetric spindle positioning in the *Caenorhabditis elegans* embryo. *Nature.* 409:630–633.
30. Grill, S. W., J. Howard, E. Schaffer, E. H. Stelzer, and A. A. Hyman. 2003. The distribution of active force generators controls mitotic spindle position. *Science.* 301:518–521.
31. Mallik, R., B. C. Carter, S. A. Lex, S. J. King, and S. P. Gross. 2004. Cytoplasmic dynein functions as a gear in response to load. *Nature.* 427:649–652.
32. Brenner, S. 1974. The genetics of *Caenorhabditis elegans*. *Genetics.* 77:71–94.
33. Panorchan, P., Y. Tseng, and D. Wirtz. 2004. Structure-function relationship of biological gels revealed by multiple particle tracking and differential interference contrast microscopy: the case of human lamin networks. *Phys. Rev. E.* 70:041906.
34. Rahman, A., Y. Tseng, and D. Wirtz. 2002. Micromechanical coupling between cell surface receptors and RGD peptides. *Biochem. Biophys. Res. Commun.* 296:771–778.
35. Fire, A. 1986. Integrative transformation of *Caenorhabditis elegans*. *EMBO J.* 5:2673–2680.
36. Berg, H. C. 1993. Random Walks in Biology. Princeton University Press, Princeton, N.J.

37. Kole, T. P., Y. Tseng, and D. Wirtz. 2004. Intracellular microrheology as a tool for the measurement of the local mechanical properties of live cells. *Methods Cell Biol.* 78:45–64.

38. Tseng, Y., J. S. Lee, T. P. Kole, I. Jiang, and D. Wirtz. 2004. Micro-organization and visco-elasticity of the interphase nucleus revealed by particle nanotracking. *J. Cell Sci.* 117:2159–2167.

39. Gupton, S. L., K. L. Anderson, T. P. Kole, R. S. Fischer, A. Ponti, S. E. Hitchcock-DeGregori, G. Danuser, V. M. Fowler, D. Wirtz, D. Hanein, and C. M. Waterman-Storer. 2005. Cell migration without a lamellipodium: translation of actin dynamics into cell movement mediated by tropomyosin. *J. Cell Biol.* 168: 619–631.

40. Strome, S. 1986. Fluorescence visualization of the distribution of microfilaments in gonads and early embryos of the nematode *Caenorhabditis elegans*. *J. Cell Biol.* 103:2241–2252.

41. Bausch, A. R., W. Môller, and E. Sackmann. 1999. Measurement of local viscoelasticity and forces in living cells by magnetic tweezers. *Biophys. J.* 76:573–579.

42. Haber, C., and D. Wirtz. 2000. Magnetic tweezers for DNA micromanipulation. *Rev. Sci. Instrum.* 71:4561–4570.